ISSN 2587-1943

# MICROHARDNESS AND MICROSTRUCTURE OF FIBER LASER WELDED S960 AND S700 STEELS

*Ö. Ekinci 1, Z. Balalan 2*

Original scientific paper

In this study, keyhole laser bead-on-plate welding of 6 mm thick high strength low alloy (HSLA) S960 steel plateand keyhole laser butt welding of 13 mm thick (HSLA) S700 steel plates were performed by using 16 kW fiber laser machine. Microhardness measurements and microstructural study on the fusion zone, heat affected zone and base material were carried out for different welding parameters that are used for welding of S960 and S700 steels. Furthermore, X-Ray Diffraction (XRD) patterns of the welded zone was performed. In laser bead on plate welding joints of S960 steels, the average microhardness value of fusion zone (FZ) is approximately 60 HV higher than that of base metal for all the welding specimens, while the microhardness value of FZ in laser butt welded joints of S700 steel is approximately 30 HV. On the other hand, microstructures of FZ consists of martensite phases, whereas both base material S960 and S700 consist of tempered martensite and strip-like martensite.

***Keywords:*** *laser welding, microhardness, microstructure, S960, S700 steels*

# FİBER LAZER KAYNAKLI S960 VE S700 ÇELİKLERİNİN MİKROYAPI VE MİKROSERTLİKLERİ

Bu çalışmada, 16 kWfiber lazer kaynak makinesi kullanılarak 6 mm kalınlığındaki yüksek dayanımlı düşük alaşımlı S960 çelik plaka yüzeyine kaynak ve 13 mm kalınlıktaki S700 çelik plakaların alın kaynağı yapılmıştır. Farklı kaynak parametreleri kullanılarak kaynak edilen S700 ve S900 çeliklerinin kaynak bölgesinin ısı tesiri altında kalan bölgesinin (ITAB) ve ana malzemenin mikroyapı ve mikrosertlik değerleri tespit edilmiştir. Ayrıca, XRD testiyle kaynak dikişindeki fazlar elde edilmiştir. S960 çeliğinin kaynaklarında (ITAB)'da kalan bölgenin sertliği yaklaşık 60 HV ve bu kaynak işlemlerinde (ITAB)'da sertlik değerinin ana malzemenin sertlik değerinden daha yüksek çıkmıştır. S700 çeliğinin alın kaynağında ITAB'ın yaklaşık 30 HV değeri elde edilmiştir. Diğer taraftan hem S960 hem de S700 çeliğinin kaynağında ITAB'ın martenzit, temperlenmiş martenzit ve şerit şeklinde fazlardan meydana gelmiştir.

***Anahtar Kelimeler****: Lazer kaynağı, mikrosertlik, mikroyapı, S960, S700 çelikleri*

## 1 Introduction

High strength low alloy (HSLA) steels have been used in a wide range of applications for years because of their great strength, toughness, weldability and strength weight ratio. For instance, these HSLA steels are used as construction elements in the shipbuilding, offshore industries, pressure vessels, the automotive industry and oil transportation pipes (Oñoro et al., 1997; Yan, et al., 2009) The use of HSLA steels as construction elements make lighter and more slender components possible and lowers setup costs without losing structural integrity (Shi and Han, 2008; Takasawa et al., 2012). Welding is a fundamental fabrication method in joining HSLA steels (Ghosh et al., 2010). Welding HSLA steels with traditional arc welding techniques produces large heat inputs in the welding zone, which leads heat affected zone (HAZ) to become soft and thus strength of welding zone decreases (Viano et al., 2000; Zhang et al., 2012). This is an important issue for high strength HSLA steels, however, this issue might be overcome via rapid water cooling. On the other hand, laser welding can be a good alternative for welding HSLA steels, which is a non-contact welding technique, tenders great welding speeds, low distortion, strong and tough joints due to its large power density and low heat inputs (Esfahani et al., 2015; Hao et al., 2015).

In this study, keyhole laser welding of S960 and S700 HSLA steels was successfully carried out without using filler wire. In order to determine the weldability of these HSLA steels, the microstructure, XRD and microhardness tests were performed and assessed.

## 2 Materials and Method

In this study, 6 mm thick HSLA steel plate (S960, Tata Steel, $\sigma_{y,min}$ is 960 MPa) was used for keyhole fiber laser bead on plate welding. The chemical composition of S960 base material is given in Table 1. Additionally, 13 mm thick HSLA steel plate (S700, Tata Steel, $\sigma_{y,min}$ is 700 MPa) was used for keyhole fiber laser butt welding. The chemical composition of S700 base material is given in Table 2. A 16 kW continuous wave fiber laser (IPG YLS-16000) was utilized for keyhole welding operations. Experimental setup for the keyhole fiber laser welding is shown in Figure 2. During welding operations, argon gas was employed for shielding the top and back surfaces of the workpieces so as to protect the molten metal from the surrounding atmosphere. Keyhole laser welding experiments were performed by applying a variety of welding speeds and laser powers. On the basis of previous published studies (Guo et al., 2017) with single pass laser welding of HSLA steels, bead on plate single pass laser weldings of 6 mm thick S960 steel was performed at welding speeds of 0.9 m min, 1.05 m min, 1.2 m min and 1.5 m min with laser powers of 4 kW, 5 kW and 6 kW, respectively. Moreover, single pass laser butt weldings of 13 mm thick S700 steel was performed at welding speeds of 0.5 m min and 0.72 m min with laser powers of 11.5 kW and 13 kW. Welding parameters are presented for S960 and S700 steels in Table 3 and Table 4. After keyhole laser welding operations, welded parts were cut from welded areas to reveal weld cross sections. The weld cross sections were ground, polished and then etched with a solution of 3% Nital for about 15 s. Weld cross sections of S960 and also S700 steel produced with different

welding parameters are given in Figure 3 and 4. In order to examine the microstructure of the welds, JEOL JMS 6510 scanning electron microscope (SEM) was used. For crystal phase identification in the fusion zone, XRD analysis was conducted **by** Rigaku Ultima IV X-Ray Difractometer machine using Cu target (λ = 1.544 Å). Micro-hardness across the welded joint was measured using a load of 100 g with a Vickers micro-hardness machine (Emco Test DuraScan). Hardness determination was implemented in the base metal, fusion zone and heat affected zone.

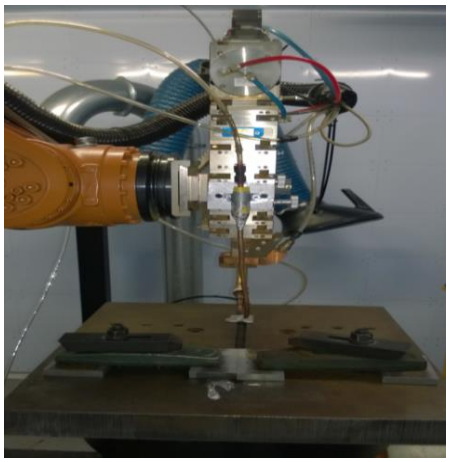

**Figure 1**. Experimental setup for keyhole fiber laser welding

## 3 Results and discussion

### Macrostructures

The weld bead of the keyhole laser bead on plate welding of S960 and butt welding of S700 HSLA steel with weld cross section presented in Figure 2. Porosity was observed in weld zone of S5 and S6 of S700 steel while undercut was observed in the weld bead of S3 and S4 of S960 steel. Weld sagging due to excessive viscosity at the bottom of S1specimen of S960 steel was also observed. On the other hand, undercut, weld sagging or porosity were not observed in the weld zone of S2 of S960 steel. Macrostructure shows that, weld bead width of S5 of S700 steel is noticeably wider than that of S6 of S700 steel because of higher heat input in the welding S5. Fusion zone (FZ), heat affected zones (HAZ) and base material (BM) can be perceptibly seen from weld cross sections in Figure 2 (a) and (b). From weld cross section of S2 for welding S960 steel in Figure 2 (a) and weld cross section of S6 for welding S700 steel in Figure 2 (b); there are two different heat affected zones occured, which are coloured as dark region representing HAZ, coarse-grained HAZ (CGHAZ) next to fusion zone (FZ) and the other heat affected zone appears as white strip far from fusion zone, that is intercritical HAZ (ICHAZ).

**Table 1**. Chemical composition of S960 steel

| Material | Elements ( mass % ) | | | | | | | | | | | | | |
|---|---|---|---|---|---|---|---|---|---|---|---|---|---|---|
| | C | Si | Mn | P | S | Al | Cr | Mo | B | Ti | Nb | V | N | Fe |
| S960 | 0.094 | 0.108 | 1.59 | 0.011 | 0.002 | 0.038 | 0.50 | 0.26 | 0.0025 | 0.027 | 0.04 | 0.047 | 0.0052 | Bal. |

**Table 2.** Chemical composition of S700 steel

| Material | Elements ( mass % ) | | | | | | | | | | | | |
|---|---|---|---|---|---|---|---|---|---|---|---|---|---|
| | C | Si | Mn | P | S | Cr | Mo | Al | Nb | V | B | Ti | Fe |
| S700 | 0.066 | 0.107 | 1.55 | 0.01 | 0.003 | 0.499 | 0.239 | 0.07 | 0.04 | 0.051 | 0.002 | 0.002 | Bal. |

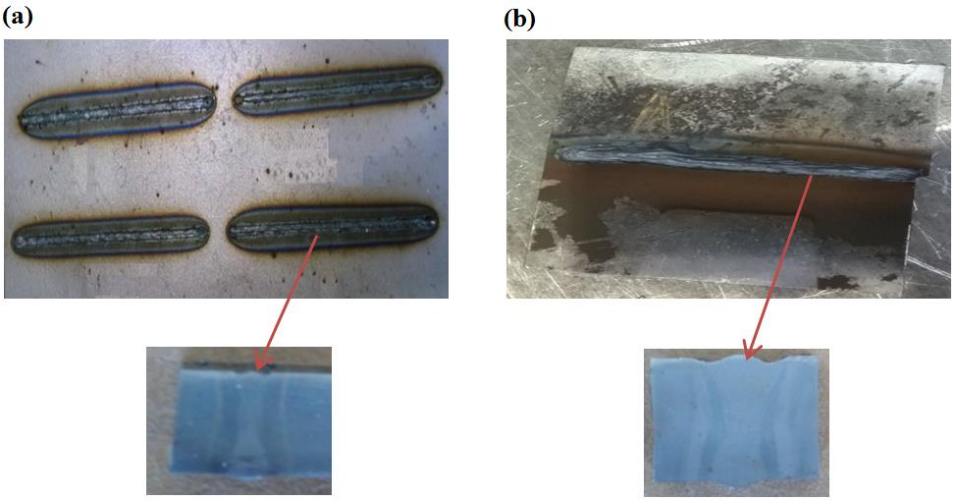


**Figure 2. (a)** Macrostructure of bead on plate weldings of S960 steel, **(b)** butt welding of S700 steel

**Table 3.** Welding parameters employed in this study for S960 steel

| No | Welding material | Thickness of material (mm) | Welding type | Laser power (kW) | Welding speed (m min) | Shielding gas |
|---|---|---|---|---|---|---|
| S1 | S960 | 6 | Single pass (Without filler material) | 4 | 0.9 | Pure argon |
| S2 | | | | 5 | 1.05 | |
| S3 | | | | 6 | 1.2 | |
| S4 | | | | 6 | 1.5 | |

**Table 4.** Welding parameters employed in this study for S700 steels

| No | Welding | Thickness of | Welding type | Laser Power | Welding speed (m | Shielding gas |
|---|---|---|---|---|---|---|
| S5 | S700 | 13 | Single pass (Without filler | 11.5 | 0.5 | Pure argon |
| S6 | | | | 13 | 0.72 | |

## Microhardness

After keyhole laser bead on plate welding of the samples with different laser power and welding speed, microhardness of base material, intercritical heat affected zone and fusion zone were measured from cross section of the welded joint across the mid-section of each sample as shwon in Figure 3. Microhardness values of base material, intercritical heat affected zone and fusion zone were presented in Figure 4 for each welded joint. From the Figure 4, it can be seen that S1 has the lowest microhardness values in the series while S4 has the highest microhardness values. In general, hardness values are greater in all FZ and HAZ when compared with base material and also the hardness of the intercritical heat affected zones is slightly higher than those of fusion zones. Although the hardness values of S2, S3 and S4 are almost nearly similar, S1 has typically lower hardness values.

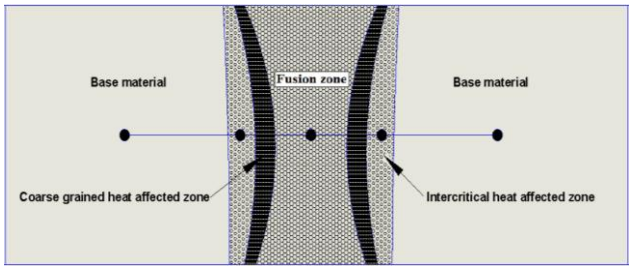


**Figure 3**. Microhardness measurement order

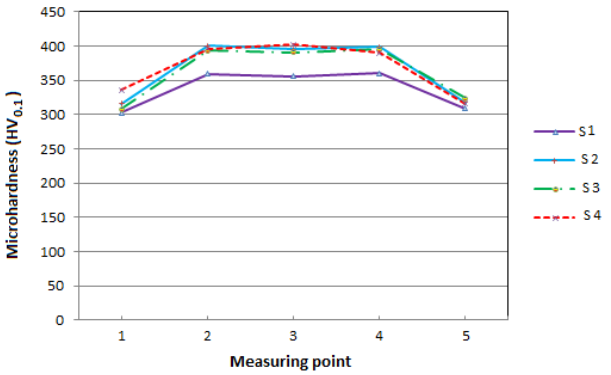


**Figure 4.** Microhardness vs. distance curve for Keyhole laser bead on plate welding of S960 steel

The reason for this could be effect of heat input since S1 has the least heat input value. According to (Guo et al., 2015), because of fast heating and cooling rates occurring in laser welding, the formation of martensite in the FZ and HAZ takes place. This leads to an increase in hardness in the FZ and HAZ. (Lee et al., 2010) determined that the yield strength for FZ and HAZ are approximately 1.2 times that of base material. Microhardness curves with respect to distance for keyhole laser butt weldings of S700 steel are shown in Figure 5. This Figure 5 expresses that the hardness of S6 is greater than S5. The reason for higher hardness in the S6 may be due to the welding speed, as S6 possesses greater welding speed. According to Tash and Gadelmola (Tash and Gadelmola, 2016), the differences in hardness are because of the low heat input and high cooling rate generated as a consequence of increase in laser welding speed. Another reason for high hardness is different phases occurring in the microstructure of FZ and HAZ.

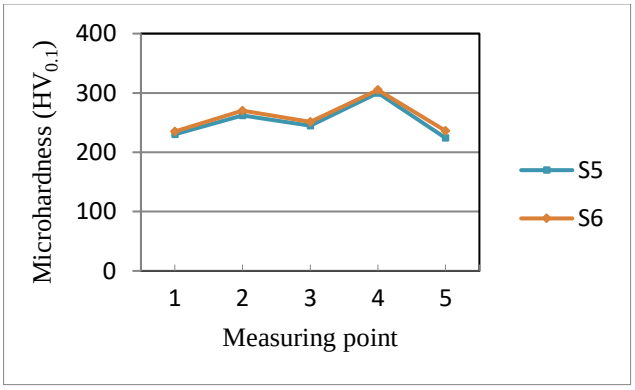


**Figure 5.** Microhardness vs distance for Keyhole laser butt welding of S700 steel

During welding process, heating and cooling events occur which cause phase transformations in base material. These phase transformations change the material properties and also volume of the material. In addition, in the welding process, phase transformations play an important role in the occurrence of residual stresses which affect mechanical properties of the material (Wang et al., 2017; Zubairuddin et al., 2017; Deng 2009).

In the welding process of steels, material is heated and melted and hence from liquid phase to alpha phase (i.e. alpha ferrite), several phase changes occur. Alpha ferrite can only dissolve in small quantity of carbon atoms and thus excessive carbon atoms is rejected to the solution. As high cooling rates occur there is no sufficient time for carbon atoms to leave rather carbon atoms are trapped and precipitate inside the alpha phase as Fe3C) and/or form solid solution phases such as bainite, widmanstaten ferrite and martensite. These martensites and carbides account for hardness and strength of weld joint (Nivas Ramachandiran, 2016).

## Microstructure

In order to determine types of phases in the microstructure after keyhole laser bead on plate welding of S960 HSLA steel and keyhole laser butt welding of S700 HSLA steel at different welding conditions, base metal, fusion zone FZ and coarse-grained heat affected zone CGHAZ were characterized by SEM (Scanning Electron Microscopy). According to Poorhaydari et al., and Lan et al., (Poorhaydari et al., 2005; Lan et al., 2012), the most significant aspects are the peak temperatures and cooling rate when assessing the microstructure of fusion zone and heat affected zone in the welded joint. The maximum temperature is observed at the CGHAZ, and hence this led grain size to increase in this sub-zone (Guo et al., 2017). The microstructure of the base material of S960 HSLA steel obtained by using SEM machine given in Figure 6. As can be seen in the Figure 6 that the base metal has elongated grains which was generated during the hot rolling process.

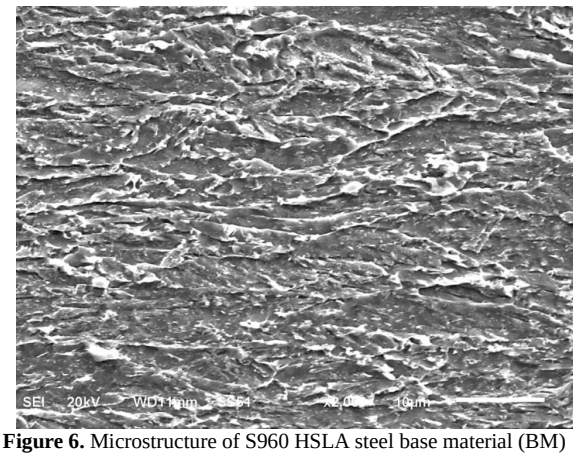

**Figure 6.** Microstructure of S960 HSLA steel base material (BM)

It is explicit from Figure 7 that the microstructure of base material (BM), fusion zone (FZ) and coarse-grained heat affected zone are different when comparing with each other. While the microstructure of FZ consists of almost completely martensite, which could be due to the rapid cooling rate, the microstructure of CGHAZ consists of a mixture of martensite and granular bainite structure. Figure 8 indicates the microstructure in the fusion zone (FZ) and coarse-grained heat affected zone (CGHAZ) for S2 after keyhole laser bead on plate welding of S960 HSLA steel. In laser welding process, the temperature in fusion zone (FZ) can be greater than melting point of the welding material, Figure 8 (a) shows only columnar grain structure formed in the FZ after melting and then solidification of FZ, whereas Figure 8 (b) shows that the microstructure in the coarse-grained heat affected zone (CGHAZ) is interlaced and equiaxed martensite, which is the result of fast cooling rate following experiencing the maximum temperature (Guo et al., 2017).

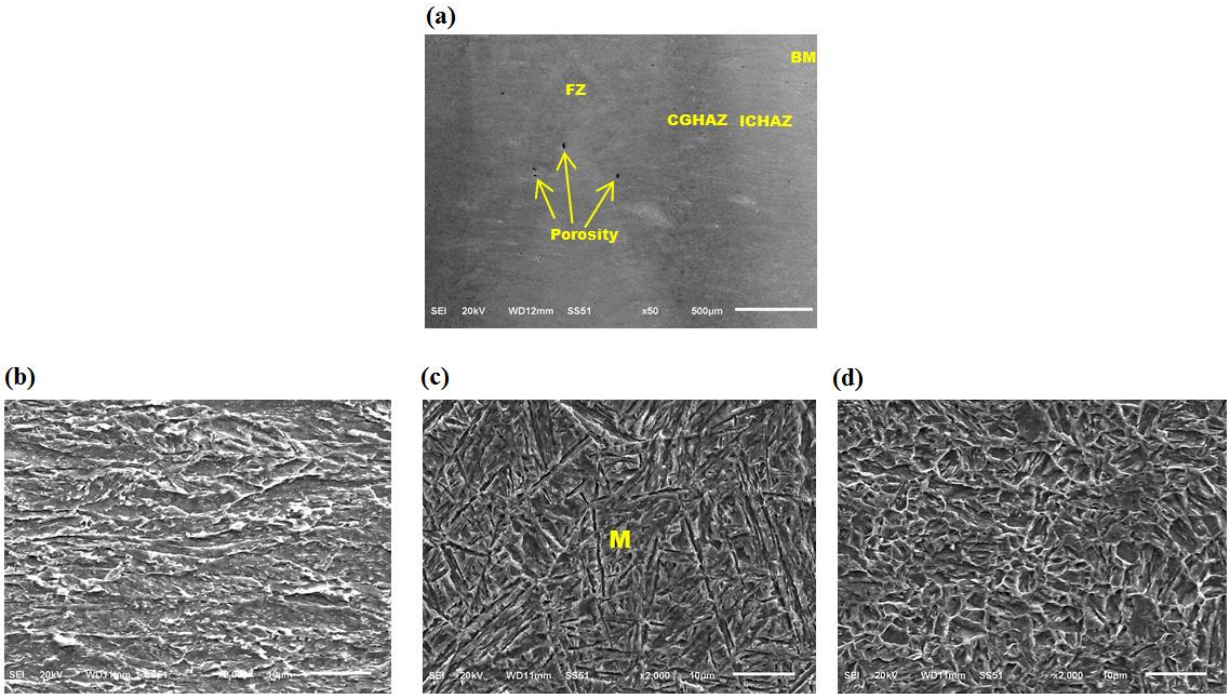


**Figure 7.** (a) The weld cross section profile of the welded S4 joint in keyhole laser bead on plate welding of S960 HSLA steel, (b) the microstructure in the base metal (BM), (c) the microstructure in the fusion zone (FZ) and (d) the microstructure in the coarse grained heat affected zone (CGHAZ) in this weld cross section profile of S4. M: Martensite

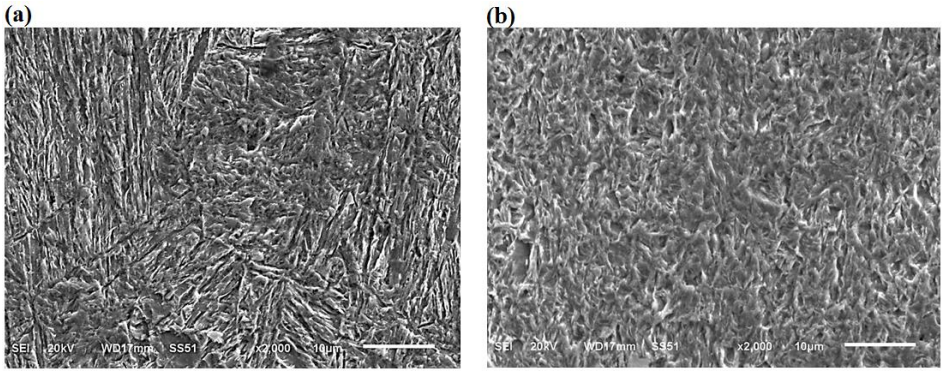


**Figure 8.** (a) Microstructure of FZ and (b) CGHAZ for keyhole bead on plate welding of S2

Figure 9 from S3 keyhole laser welding of S960 HSLA Steel presents the boundary line between coarse-grained heat affected zone (CGHAZ) and intercritical heat affected zone (ICHAZ). The boundary line can be seen clearly. From Figure 9, it is clear that grain size of CGHAZ is bigger than that of ICHAZ and color of CGHAZ is dark while color of ICHAZ is white. (Microstructures have been misinterpreted please check CCT diagrams and literature)

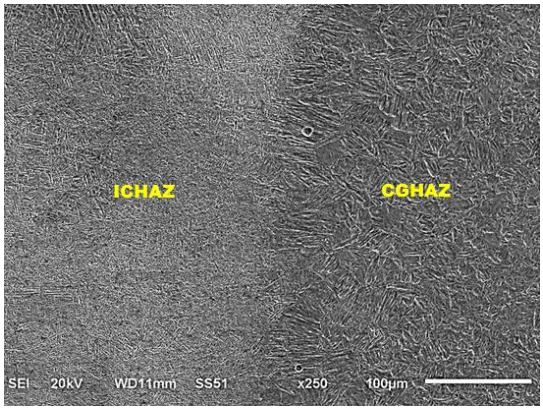


**Figure 9.** The transition from CGHAZ to ICHAZ in S3

Figure 10 shows the microstructure of the base material (BM) of S700 HSLA steel obtained by using SEM machine. Figure 10 exhibits that the base material (BM) is formed from partially tempered martensite and bainitic structure From the weld cross section profile of welded S7 joint, fusion zone (FZ) and and coarse grained heat affected zone (CGHAZ) can be clearly seen and also the boundary between FZ and CGHAZ is obvious in Figure 11 (a). The microstructure of FZ in Figure 11 (b) consists of mostly martensite laths and some lower bainite. Fig. 11 (c) represents CGHAZ' microstructure and its grain boundaries can be seen clearly. When FZ is compared with CGHAZ in terms of mcirostructure, there are more martensite laths in FZ than CGHAZ and grain sizes of CGHAZ are larger than those of FZ. Figure 12 demonstrates the welded S6 joint' microstructure in keyhole laser butt welding of S700 HSLA steel. This microstructure has interlaced martensite phases and bainite phases. XRD patterns of the welded joints of HSLA S960, S700 and the base materials were presented in Figure 13 and Figure 14 respectively. XRD patterns revealed that the base materials and the weld joints were completely consisted of α ferrite phase in the microstructure of fusion zone was observed. Martensite has a smaller lattice parameter than that of alpha ferrite and therefore the martessite peaks are not visible with wavelength of Cu target (1.544Å), unless the phase itself was tempered and recovered following the welding, transforming into alpha ferrite in structure but has a recopvered structure in appearance.

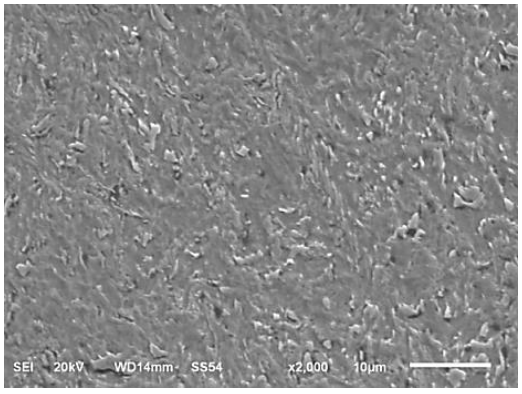


**Figure 10.** Microstructure of S700 HSLA steel base material

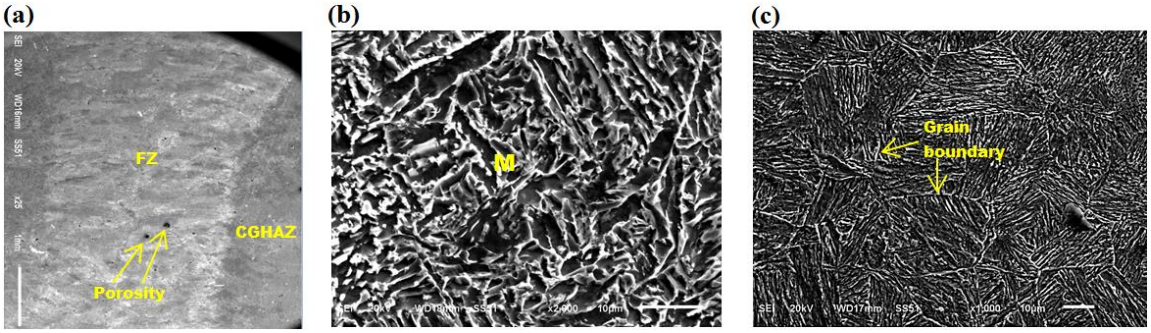


**Figure 11.** (a) The weld cross section profile of welded S6 joint in keyhole laser butt welding of S700 HSLA steel, (b) the microstructure in the fusion zone (FZ) and (c) the microstructure in the coarse grained heat affected zone (CGHAZ) in this weld cross section profile of S6. M: Martensite

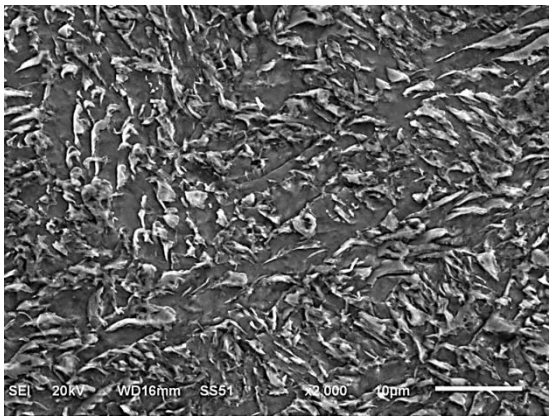


**Figure 12.** The microstructure of the FZ of S6

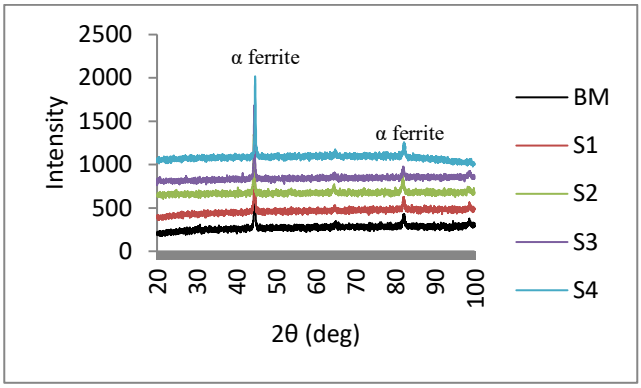


**Figure 13.** XRD patterns of laser welded joints for S960

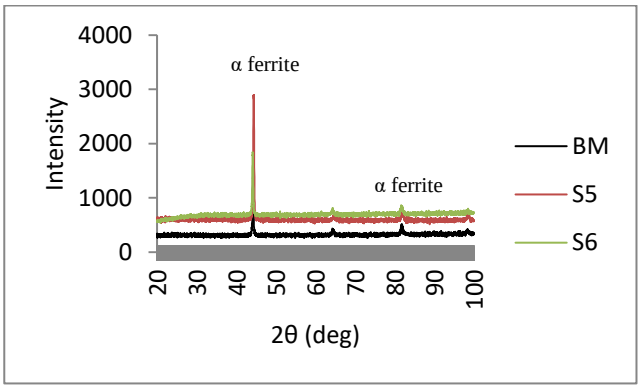


**Figure 14.** XRD patterns of laser welded joints for S700

## 4 Conclusions

Mechanical properties and microstructures of keyhole laser bead on plate welding joints of S960 HSLA steel and butt welding joints of S700 HSLA steel were investigated. The main conclusions were presented below:

(1) The average microhardness value of the FZ is approximately 395 HV while the value of BM is 320 HV in laser bead on plate welding joints. It was found that microhardness value increases gradually from BM to FZ. The biggest value is on the zone which is between CGHAZ and ICHAZ. S4 has the highest microhardness values in S960 while S6 is in S700.

(2) Maximum porosity was observed in the weld bead of S4 and S6. These pores can reduce weld strength.

(3) It was determined that the microstructure changes across the welding joint. The microstructure of BM, FZ and CGHAZ are different from each other for each laser welding condition. It was revealed that in general, in FZ and CGHAZ, the microstructure is composed of martensite and tempered martensite which result in increasing microhardness in FZ.

(4) From examining XRD patterns, it was confirmed that there are not much differences in the microstructure of FZ and CGHAZ due to similar cooling rates occuring in the weld zone.

## Acknowledgment

The authors are grateful to The University of Manchester for enabling to perform experiments. Also, The authors are grateful to Firat University and Bingol University for providing microhardness measuring device and microstructure measuring device.

## 5 References

Deng D, 2009. FEM prediction of welding residual stress and distortion in carbon steel considering phase transformation effects Mater Des, 30, pp. 359-366

Esfahani MRN, Coupland J, Marimuthu S, 2015. Numerical simulation of alloy composition in dissimilar laser welding, J. Mater. Process. Technol. 224, 135–142.

Ghosh M, Kumar K, Mishra RS, 2010. Analysis of microstructural evolution during friction stir welding of ultrahigh-strength steel, Scr. Mater. 63, 851–854.

Guo W, Li L, Dong S, Crowther D, Thompson A, 2017. Comparison of microstructure and mechanical properties of ultra-narrow gap laser and gas-metal-arc welded S960 high strength steel, Volume 91, April 2017, Pages 1-15

Guo W, Crowther D, Francis JA, Thompson A, Liu Z, Li L, 2015. Microstructure and mechanical properties of laser welded S960 high strength steel, Materials and Design 85, 534–548.

Hao K, Li G, Gao M, Zeng X, 2015. Weld formation mechanism of fiber laser oscillating welding of austenitic stainless steel, J. Mater. Process. Technol. 225, 77–83.

Lan L, Qiu C, Zhao D, Gao X, Du L, 2012. Analysis of microstructural variation and mechanical behaviors in submerged arc welded joint of high strength low carbon bainitic steel, Mater. Sci. Eng. A 558, 592–601.

Lee BS, Kim MC, Yoon JH, Hong JH, 2010. Characterization of high strength and high toughness Ni–Mo–Cr low alloy steels for nuclear application, Int. J. Press. Vessel. Pip. 87, 74–80.

Oñoro J, Ranninger C, 1997. Fatigue behaviour of laser welds of high-strength low-alloy steels, J. Mater. Process. Technol. 68, 68–70.

Poorhaydari K, Patchett BM, Ivey DG, 2005. Estimation of cooling rate in the welding of plates with intermediate thickness, Weld. J. 84, 149–155.

Ramachandiran N, Quora, Why do metals get harder on welding, https://www.quora.com/Why-do-metals-get-harder-on-welding

Shi Y, Han Z, 2008. Effect of weld thermal cycle on microstructure and fracture toughness of simulated heat-affected zone for a 800 MPa grade high strength low alloy steel, Journal of Materials Processing Technology.207:30-9.

Takasawa K, Ikeda R, Ishikawa N, Ishigaki R, 2012. Effects of grain size and dislocation density on the susceptibility to high-pressure hydrogen environment embrittlement of high-strength low-alloy steels, International Journal of Hydrogen Energy.37:2669-75.

Tash MM, Gadelmola KM, 2016. Effect of welding speed on the micro-hardness and corrosion resistance of similar laser welded (304 304) stainless steels and dissimilar (304 A36) stainless and carbon steels, Advanced Materials and Structural Engineering, ISBN 978-1, 138-02786-2.

Viano DM, Ahmed NU, Schumann GO, 2000. Influence of heat input and travel speed on microstructure and mechanical properties of double tandem submerged arc high strength low alloy steel weldments, Sci. Technol. Weld. Join. 5, 26–34.

Wang Q, Liu X.S, Wang P, Xiong X, Fang H.Y, 2017. Numerical simulation of residual stress in 10Ni5CrMoV steel weldments J Mater Process Technol, 240, pp. 77-86

Yan W, Zhu L, Sha W, Shan Y, Yang K, 2009. Change of tensile behavior of a high-strength low-alloy steel with tempering temperature, Mater. Sci. Eng. A 517, 369–374.

Zhang C, Lu P, Hu X, Song X, 2012. Effect of buffer layer and notch location on fatigue behavior in welded high-strength low-alloy, J. Mater. Process. Technol. 212, 2091–2101.

Zubairuddin M, Albert S.K, Vasudevan M, Mahadevan S, Chaudhari V, Suri V.K, 2017. Numerical simulation of multi-pass GTA welding of grade 91 steel J Manuf Process, 27, pp. 87-97

**Authors' addresses**

***Omer Ekinci 1***
Faculty of Engineering and Architecture,
Bingol University, Bingol-Turkey
oekinci@bingol.edu.tr

***Zulkuf Balalan 2***
Faculty of Engineering and Architecture,
Bingol University, Bingol-Turkey
zbalalan@bingol.edu.tr